Effect of Sodium Lauryl Sulfate on the Properties of the Electrodeposited Invar Alloy

Ji-Han Kwak, In-Gyeong Kim, Yong-Bum Park and Se-Eun Shin *

Department of Advanced Materials Engineering, Sunchon National University, Suncheon 57922, Republic of Korea; wlgks8929@naver.com (J.-H.K.); igkim@scnu.ac.kr (I.-G.K.); ybpark@scnu.ac.kr (Y.-B.P.)
* Correspondence: shinsen@scnu.ac.kr; Tel.: +82-061-750-3553

Abstract: In the OLED display manufacturing process, a fine metal mask (FMM) is used for the RGB side-by-side in precise positions. An Invar alloy with exceptionally low thermal expansion was used as the FMM material to prevent the deformation of the FMM by heat during the deposition process. The thickness of the FMM must be reduced to less than 10 microns to manufacture high-resolution OLED displays, making it essential to apply a bottom-up electrodeposition process. Moreover, controlling the interfacial energy of the cathode substrate and the electrolyte is necessary to achieve ion electrodeposition and peeling of the ultra-thin Fe-Ni plated on the cathode substrate during electrodeposition. Therefore, this study investigated the effect on the properties of the electrodeposited Fe-Ni alloy by controlling the amount of SLS content, which acts as a surfactant. The amount of SLS content was maintained in the range of 0 to 1 g/L, and the composition homogeneity, microstructure, and surface defects of the electrodeposited Fe-Ni alloy were investigated. Under low pH conditions, the composition was insignificantly changed depending on the difference in the amount of SLS content, and a uniform composition was observed. The findings of this research offer valuable insights for optimizing the electrodeposition process, which is crucial for producing high-resolution OLED displays with ultra-thin FMM, advancing display technology.

Keywords: electroforming; Fe-Ni alloy; Invar; microstructure; sodium lauryl sulfate

1. Introduction

The use of FMM (fine metal mask) in the organic light-emitting diode (OLED) display process necessitates the selection of materials that can withstand heat during the deposition process, and a suitable material used for this process is the Fe-Ni alloy [1]. However, traditional pyrometallurgy techniques for manufacturing the Fe-Ni Invar alloy face technical limitations, particularly in achieving a thickness of less than 20 μm [2]. For rolled Invar alloy film, it was difficult to obtain a higher resolution than quarter high definition (QHD) because the thickness was difficult to reduce. Consequently, the production method was changed from pyrometallurgy to electroforming plating, enabling the production of an Fe-Ni alloy. In addition, it provides the possibility of precise processing option with enhanced mechanical properties and thermal dimensional stabilities. It allows high dimensional accuracy and degrees of freedom to produce the Fe-Ni alloy. The electroplating method, as opposed to the pyrometallurgy method, is a method of stacking samples like the lamination method, which helps to secure a material with a thickness of approximately 10 μm [3]. The electrodeposition method normally processes the room temperature and it leads to savings by increasing economies of scale in the manufacturing of Fe-Ni alloy production compared to the conventional rolling process. Although the control of electrodeposition conditions has been challenging, the possibility of successful fabrication results of the Fe-Ni alloy has been reported [3–7].

Meanwhile, the coefficient of thermal expansion (CTE) of the samples produced by electroplating was higher than that of the samples produced by pyrometallurgy. The

samples made by pyrometallurgy had a face-centered cubic (FCC) structure, and the samples made by electroforming had an FCC structure. This result was observed because it consists of a metastable body-centered cubic (BCC) structure or a mixture of FCC and BCC structures [4–6]. Because the crystal structure is different, the CTE is different, and when heat treatment is performed, a lower CTE can be obtained with the electroplating method than the pyrometallurgical method [1]. There are various ranges of CTE values depending on the Ni contents; primarily materials containing 36 to 41 wt% of Ni have been reported to exhibit a low CTE [7]. Therefore, the most successful fabrication method of the Fe-Ni alloy is electrodeposition, which can achieve high-quality color images in such displays. For electrodeposition, the influence of additives in the electrolyte on the composition of electrodeposited Fe-Ni alloys is the key parameter. Therefore, several researchers reported the effect of the various additives on the Fe-Ni alloy fabricated using electrodeposition [3–6].

This study explores the characteristics and composition of the Fe-Ni Invar alloy fabricated by the electroplating method, which are influenced by the additives added to the plating solution during the electroplating process. The key additives added to the plating solution include $FeSO_4 \cdot 7H_2O$, $NiSO_4$, $NaCl$, H_3BO_3, $C_7H_4NNaO_3 \cdot 2H_2O$, and sodium lauryl sulfate (SLS) $(CH_3(CH_2)_{11}OSO_3Na)$ [8,9]. Other conditions include current density, temperature, stirring speed (rpm), Ni plates as anodes, and stainless steel (STS 316) as cathodes. This study investigates samples with varying Ni contents (33, 36, and 42 wt%) prepared with varying SLS contents, which is one of the common additives in the plating solution production process [10]. SLS is added as a surfactant in the plating solution, where it serves to make the sample glossy as a mirror by uniformly dispersing the solution and ensuring consistent deposition [10–12]. The experiment was conducted with varying current density (8–14 and 10–16 mA/cm^2) and pH (2.4 and 2.8) values of the plating solution [13–16].

2. Experimental Procedures

2.1. Electroplating Process

A modified Ni plating bath (sulfate bath) was used to prepare a 4 L Fe-Ni alloy plating bath, and details of the bath composition and plating conditions are listed in Tables 1 and 2. The plating bath contained $Fe_2SO_4 \cdot 7H_2O$ (ferrous sulfate), $NiSO_4$ (nickel sulfate) as metal sources, sodium chloride (NaCl) and H_3BO_3 (boric acid) as a pH buffer, and $C_7H_4NNaO_3 \cdot 2H_2O$ (saccharin) as a surface active agent.

Table 1. Details of bath composition.

	$Fe_2SO_4 \cdot 7H_2O$ (Ferrous Sulfate)	$NiSO_4$ (Nickel Sulfate)	NaCl (Sodium Chloride)	H_3BO_3 (Boric Acid)	$C_7H_4NNaO_3 \cdot 2H_2O$ (Saccharin)
Contents (g/L)	85	97	30	25	2.6

Table 2. Details of electrodeposition processing parameters based on the SLS content.

pH	Current Density (mA/cm²)	SLS Contents (g/L)	pH	Current Density (mA/cm²)	SLS Contents (g/L)
2.8	8–14	0	2.4	8–14	0
		0.1			0.1
		0.2			0.2
		0.5			0.5
		1			1
	10–16	0		10–16	0
		0.1			0.1
		0.2			0.2
		0.5			0.5
		1			1

Each reagent was dissolved in distilled deionized water to prepare the plating bath.

Saccharin sodium is well-known as a stress reducer in Ni plating [13] and is also indispensable to obtain the crack-free Fe-Ni Invar alloy electrodeposits with a shiny and smooth surface morphology consisting of nanograins [16]. There are various combinations of the electroplating conditions, pH (2.4 and 2.8), and current density for the plating bath, such as a low density of 8–14 A/cm^2 and a high density of 10–16 A/cm^2, respectively. To achieve meaningful feasibility, the pH conditions were fixed at 2.4 and 2.8, because under pH 2.4 conditions, the sample surface remained constant without being affected by the increased amount of SLS contents. The range of the current density under two conditions allows electroplating to proceed well and obtain an intact sample considering delamination issues. A stainless steel (STS316, Steel&I, Seoul, Republic of Korea) wafer 50 × 150 mm^2 was used as the cathode, and a pure Ni sheet was used as the anode. The plating bath was maintained at 55 °C for 2.5 h in a 4 L electrolysis cell, and the magnetic stirrer at 30 RPM with a magnetic spin bar was attributed to the achieved homogeneity of the plating solution. After measuring the initial pH, sulfuric acid (H_2SO_4) was added to lower the pH, and the cathode and anode were fixed to the simulator, placed in the plating solution, and an electric current was applied to secure the sample. The thickness of the electrodeposition layer was proportional to the applied current time. In this experiment, the applied current was 5 min at the initial current density and 60 min, which resulted in a sample with a thickness of less than 10 μm.

2.2. Material Characterizations

After electrodeposition, the electrodeposited films were mechanically removed from the STS316 substrate. The thickness of the specimens was 9–11 μm and 46 × 138 mm^2. The microstructure of the electrodeposited Fe-Ni Invar alloys was investigated using a field emission scanning electron microscope (SEM, JSM-7100F, JEOL, Tokyo, Japan) equipped with detectors (EDAX, Mahwah, NJ, USA) for electron backscatter diffraction (EBSD) and energy dispersive X-ray spectroscopy analyses. X-ray diffraction (D8 Discover, Bruker, Billerica, MA, USA) was used to identify the phases of the IMCs with a Cu Kα radiation source (λ = 1.5405 Å) and an uninterrupted scan modem with a scan rate of 0.05°/s and a range of 2θ (30–90°). The specimens were prepared for SEM analysis by polishing with a 1 μm diamond suspension. The CTEs of these electroformed sheets were measured in the temperature range from 298 to 333 K (25–60 °C) using a thermo-mechanical analyzer (TMA402F3, Netzsch, Selb, Germany). The sheet dimensions were 10 mm × 20 mm, and the tests were performed using a 0.05 N load. The measurement was conducted in a high purity Ar gas with a flow rate of 0.5 bar in order to avoid oxidation of the sample and the temperature was increased at a rate of 20 °C/min. These measurement conditions are used by almost all OLED FMM makers. The CTE measurements were performed on the samples with thicknesses of 8 μm and through-thickness compositional errors below 1.0 wt%.

3. Results and Discussion

Among the electroplating process conditions, $Fe_2SO_4·7H_2O$ and $NiSO_4$ were set as invariant using a 10 μm thick Invar thin film fabricated using the electroplating method, and the microstructural evolution of the specimens as a function of SLS contents was analyzed using EBSD analysis, as shown in Figure 1. The phase colors were coded by Fe-36Ni as red and α-ferrite as green in the phase maps.
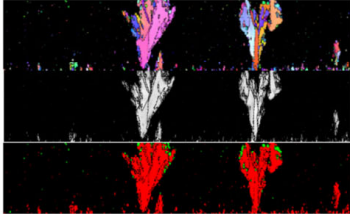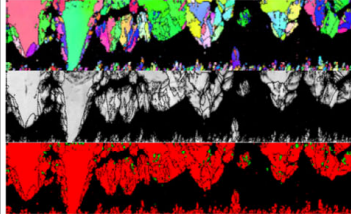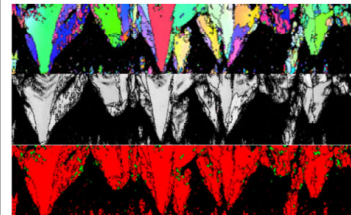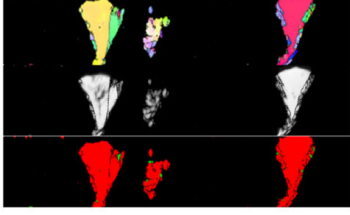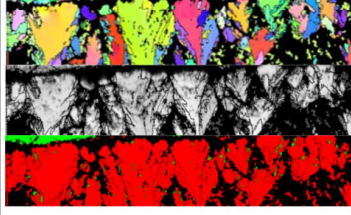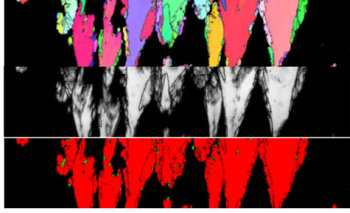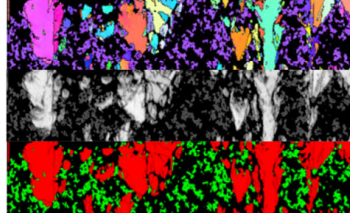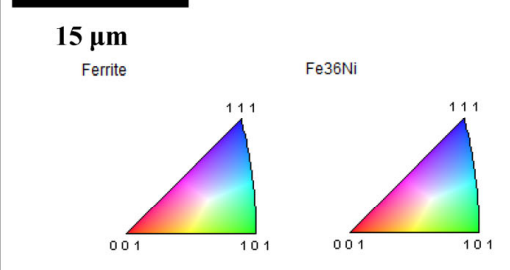
Figure 1. Typical electron backscatter diffraction (EBSD) data containing inverse pole figure (IPF) maps, image quality (IQ) maps, and phase fractions, and specimen surfaces at varying sodium lauryl sulfate (SLS) contents (g/L) at pH 2.8; (**a**,**b**) 0, (**c**,**d**) 0.1, (**e**,**f**) 0.2, (**g**,**h**) 0.5, and (**i**) 1.

White rust typically occurs on the surface of an electroplated specimen, which is a phenomenon that appears as a blurry surface caused by the appearance of α (bcc) phase columns in the microstructure, leading to surface curvature. The area of white rust expands depending on the SLS content in the current density range of $8\text{–}14\,\text{mA/cm}^2$. Figure 1a,b show the electroplated samples without SLS. The surfaces of these samples exhibited imperfections and holes due to the absence of SLS in the plating solution, leading to the retention of impurities on the surface during plating, resulting in surface inhomogeneity. Figure 1c,d show the surface and EBSD analysis results of the samples with varying current densities but the same SLS content. To confirm the microstructures according to the electrodeposition, cross-sectional areas of the samples were prepared. The electrodeposited samples with a high current density showed more severe white rust than those with a low current density. Consequently, the grain morphology showed a visible difference, as shown in the phase maps. The more severe the white rust phenomenon, the more grain growth that occurs during the electrodeposition. Therefore, samples fabricated under the current density of $10\text{–}16\,\text{mA/cm}^2$ and SLS content of 0.2 g/L at pH 2.8 with a large amount of grains were detected as shown in Figure 1f.

In the current density range of $10\text{–}16\,\text{mA/cm}^2$, the white rust occurred on the whole surface of the specimen regardless of the amount of SLS content, and in the case of SLS contents of 1 g/L at the current density of $10\text{–}16\,\text{mA/cm}^2$, a slight peeling occurred at the edge, as shown in Figure 1h (as displayed in the yellow circle). A slight peeling with a crack can be observed; it usually occurs for severe white rust or very high current densities [17]. When cracks occur in the sample, it may peel off on its own during electroplating, causing the plating solution to flow into the back of the sample, which may cause significant contamination of the sample surface with the plating solution. Ultimately, stains may form on the sample surface, or in severe cases, oxidation may occur, requiring prevention.

EBSD analysis was performed, comparing Figure 1c,e,g to thoroughly examine the white rust process. The phenomenon becomes notably more significant as the amount of SLS content increases. The effect of SLS content as a surfactant facilitates relaxation of the interface between the plating solution and the cathode and reduces the difference in surface tension at the solid–liquid interface, allowing the liquid to easily penetrate into the solid [11].

Figure 2 shows the concentration profiles along the thickness direction for different SLS contents at pH 2.8. The composition of the electrodeposited samples consisted of Ni contents at or below 30 wt.%, and as the amount of SLS content increases, the electrodeposition composition decreases, indicating a relation to the broadening of the white storage strain phenomenon. The large difference in elemental composition on the electrodeposited surface is attributable to the columnar structure that appears during the electroplating process. The columnar structure refers to pillar-shaped grains that form during the electroplating process, and their growth during the electrodeposition process was confirmed by EBSD analysis. Additionally, it can be assumed that the electrodeposition composition was low, owing to the growth of the columnar structures. As shown in Figure 2c,e,g, unlike the other samples, a uniform elemental composition was measured at the center of the samples. In particular, in Figure 1c, the thickness compositional gradient of all areas, except the electrodeposition composition, was measured uniformly. For current densities ranging from 8 to $14\,\text{mA/cm}^2$, the thickness compositional graph exhibits less uniformity compared to the current density range of $10\text{–}16\,\text{mA/cm}^2$, which is attributable to the wider white rust region. The wider the white rust region, the less uniform the composition by thickness is, as shown in Figure 2i.
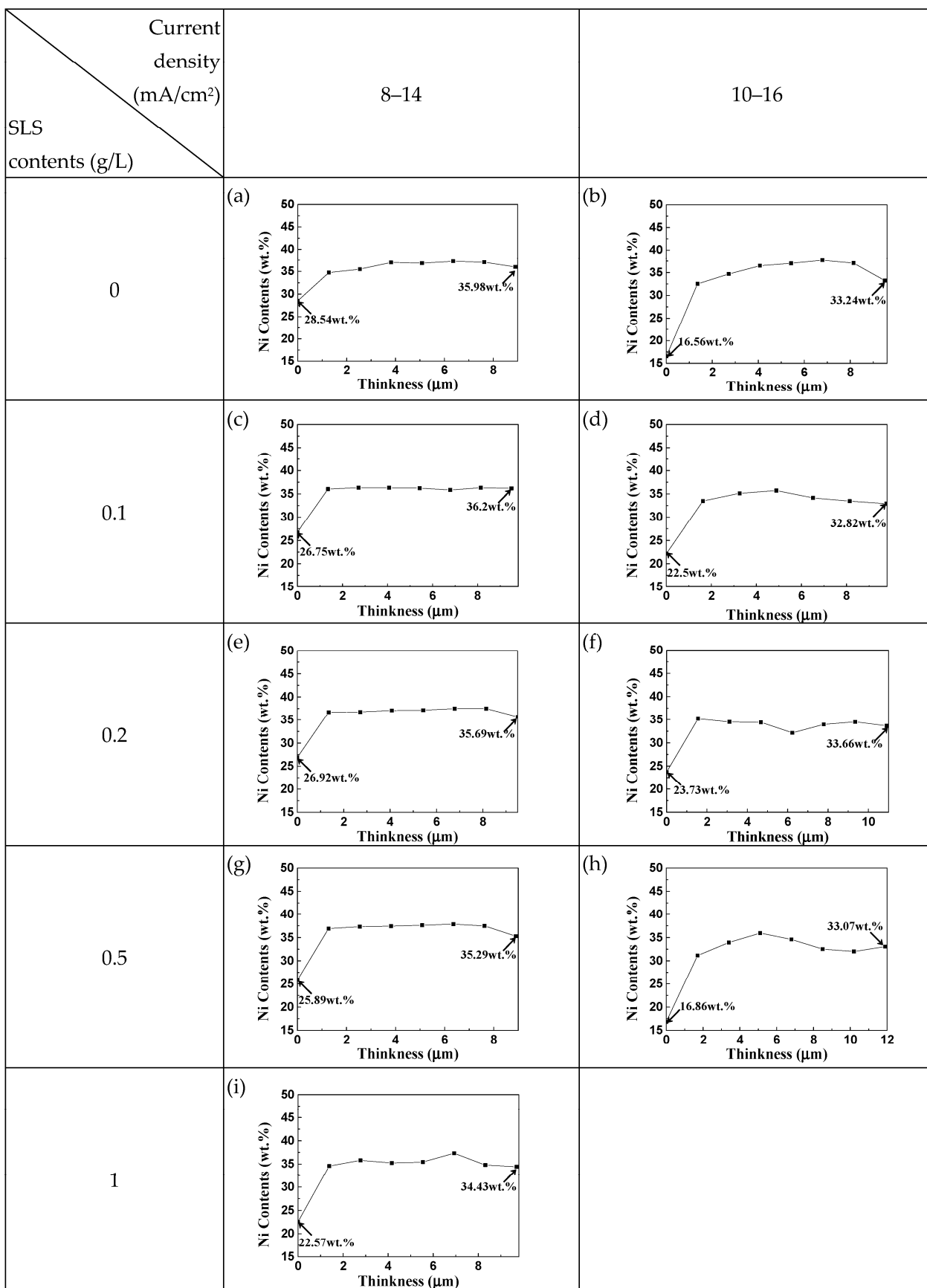
Figure 2. The concentration profile along the thickness direction at varying SLS contents (g/L) at pH 2.8; (**a**,**b**) 0, (**c**,**d**) 0.1, (**e**,**f**) 0.2, (**g**,**h**) 0.5, and (**i**) 1.

Under electroplating conditions with a current density of 10–18 mA/cm^2, the Ni content exhibits non-uniform distribution, resulting in very low electrodeposition compositions, as shown in Figure 2b,h. Both samples displayed holes and cracks on the surface, causing plating solution ingress and sample contamination, which contributed to the lower electrodeposition composition. The average sample thickness was measured to be 10–11 μm, and the amount of SLS content did not affect the thickness of the sample. However, when comparing the current density, the average thicknesses were 9.6 and 11 μm for the current densities of 8–14 mA/cm^2 and 10–16 mA/cm^2, respectively. Thicker layers were fabricated at a relatively high current density due to the increased Ni deposited in the samples. However, an increase in the amount of Ni deposited in the samples results in thicker samples, and more Ni is detected in samples prepared at relatively low current densities. This result is attributed to the fact that, although the amount of nickel electrodeposited on the cathode is large, the density of the nickel electrodeposition layer is low and the electrodeposition surface state changes irregularly, resulting in a lower Ni composition than the low current density. In addition, the density of the Ni electrodeposition layer was low, resulting in low composition uniformity under high current density conditions. Moreover, the white rust occurs severely at high current densities, attributed to the deteriorated density of the Ni electrodeposited layer causing a rough surface. Similarly, the non-uniformity observed in the compositional profile of the samples with severe white rust could be attributed to the degradation of the density of the Ni electrodeposition layer. Consequently, a higher current density or increased SLS content led to more severe white rust on the sample surface, accompanied by the non-uniform Ni composition. This result is primarily due to the changes in the irregular surface condition resulting from the decreased density of the nickel electrodeposition layer [17].

Figure 3 shows the surface and compositional gradient of the samples at pH 2.4 using the same electroplating process. In comparison to the pH 2.8 condition, mild white rust formed at current densities of 8–14 mA/cm^2, and for the current densities of 10–16 mA/cm^2, approximately 2 cm of white rust was observed from the edge to the center. The white rust occurred on the sample surface as the amount of SLS content increased at a current density of 8–14 mA/cm^2. At pH 2.4, white rust did not form with increasing SLS content, and the surface remained smooth. The composition by thickness shows a uniform distribution and a small white rust region. Comparing the surface conditions of the samples to high pH conditions, less white rust formed at a current density of 8–14 mA/cm^2. Increasing the amount of SLS content intensified the white rust under low current density and high pH conditions but had no effect on bleaching under high current density and low pH conditions.

Even at a current density of 10–16 mA/cm^2, a difference in white rust compared to high pH conditions was evident, highlighting the influence of pH on the sample surface despite the same current density and SLS content. In samples where the white rust did not form, a uniform composition was measured. In Figure 3, a relatively white rust-free surface was deposited on the sample at a current density of 8–14 mA/cm^2, and the sample was deposited with a clean surface without change despite the varying SLS content. Additionally, in a sample deposited with a current density of 10–16 mA/cm^2 in Figure 1d,f,h, less white rust occurred, indicating that low pH conditions can further suppress the white rust phenomenon. Regarding electrodeposition composition, overall, the samples have higher Ni contents compared to 2 wt%, with the electrodeposition composition exceeding 30 wt% of Ni. This composition was higher than that observed at pH 2.8 conditions, highlighting the higher composition levels at low pH.
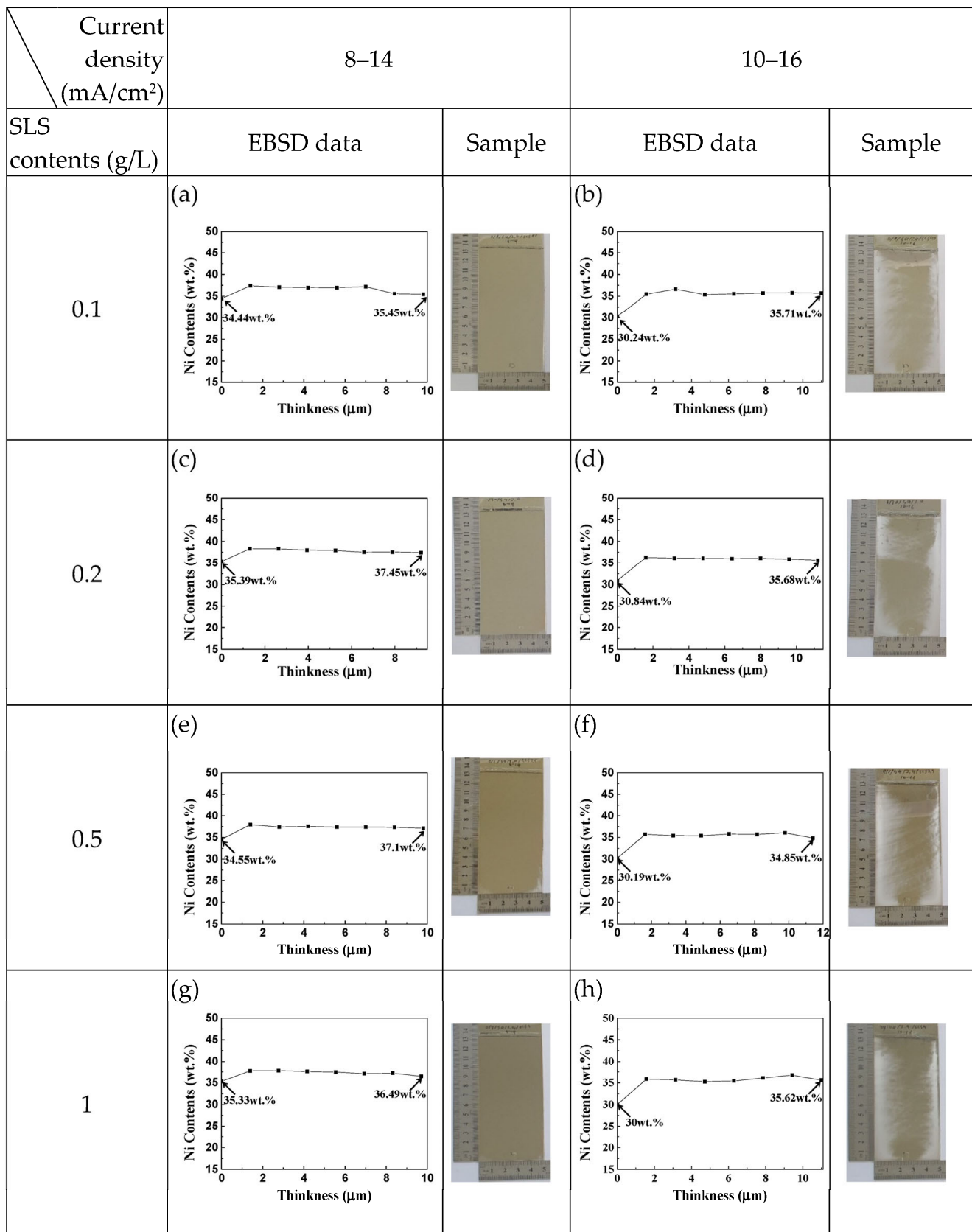
Figure 3. The concentration profile along the thickness direction at varying SLS contents (g/L) at pH 2.4; (**a**,**b**) 0.1, (**c**,**d**) 0.2, (**e**,**f**) 0.5, (**g**,**h**) 1.

In Figure 3, at pH 2.4, a homogeneous composition was obtained with a standard deviation in composition in the thickness direction of 0.4 or less under all SLS addition conditions. A mirror-grade surface was obtained at a current density of 8–14 mA/cm^2, but white rust appeared when the current density increased, which was minimally affected by the amount of SLS content. With an increase in the amount of SLS content, no apparent changes were observed in the sample, although the white rust area increased, and the composition remained relatively stable, indicating that SLS has no effect on the sample at pH 2.4. Under pH 2.4 conditions, the white rust on the sample surface can be suppressed by the difference in current density, regardless of the amount of SLS content. Overall, the amount of SLS added does not have a significant effect on the sample surface or composition under low pH conditions. Samples with a clean surface without white rust exhibited a low current density of 8–14 mA/cm^2. At a current density of 10–16 mA/cm^2, white rust formed in some parts, and the uniformity of the composition did not deteriorate because whitening did not occur throughout the sample. Increasing the amount of SLS content causes white rust on the sample surface at pH 2.8. In this experiment, under a low current density of 8–14 mA/cm^2, the white rust progressed from the edge of the sample to the center as the amount of SLS content increased. Meanwhile, as the columnar structure growth progressed, the Ni composition decreased by 2 wt% Ni. Therefore, increasing the amount of SLS added decreases the Ni composition. Consequently, a more uniform composition was obtained under the abovementioned conditions than at pH 2.8.

The EBSD results indicate that the samples containing nanosized grains were not detected, and only a few grains were possibly detected. EBSD analysis of the samples is shown in Figures 3a,b,g,h and 4. When the samples were fabricated with SLS contents of 1 and 2.5 g/L, similar results were observed, where either no meaningful results could be obtained or only a few fine grains were measured. Therefore, the samples electroplated at the highest and lowest amounts of SLS contents were compared. Although white rust formed in the electroplated samples (Figure 3b,h), it can be assumed that the reason the grain size was not measured in EBSD was due to causes other than white rust, related to the columnar structure. This conclusion is drawn from the fact that, despite a similar shape to the surface of the sample, as shown in Figure 1c, there is a difference in the EBSD analysis results. If the phenomenon were solely due to white rust, the columnar structure should have been visible, but since it is not, the white rust is attributed to other causes.

The relative change in specimen length ($\Delta L/L_0$) was measured as a function of temperature (T) and the CTEs of the electrodeposited samples is shown in Figure 5. The CTE, α, was obtained by differentiation of $\Delta L/L_0$ with respect to temperature:

$$\alpha = \frac{d}{dT}\left(\frac{\Delta L}{L_0}\right)$$

As mentioned in the experimental procedures, the measurement conditions for CTE were used by almost all the OLED FMM makers; therefore, the CTE values of the samples are defined at 60 °C according to the OLED processing temperature. Although the absolute values of the CTE are still higher than the expected value for the well-known Invar alloy, it is sufficient for a relative comparison of the SLS contents for electrodeposition. From our results at 60 °C, the sample without white rust, which was fabricated under the SLS contents of 1 g/L at a current density of 8–14 mA/cm^2 and pH 2.4, shows the lowest CTE value of $9.101 \times 10^{-6}/°C$ among the samples. The highest CTE value of $9.851 \times 10^{-6}/°C$ is for the sample with white rust overall, which was fabricated under the SLS contents of 0.1 g/L at a current density of 8–14 mA/cm^2 and pH 2.4. The difference between the CTE values resulted from the microstructures. When the sample had nanostructured grains, it presented a high CTE value. In addition, due to the sample having a low CTE value, it contained columnar structures. The samples without white rust showed lower values of $9.101 \times 10^{-6}/°C$, which is a 7.7% decrease compared to that of the samples with white rust. From the results, electrodeposition without white rust has succeeded and additional treatment for the absolute CTE value near zero will be carried out in future works.
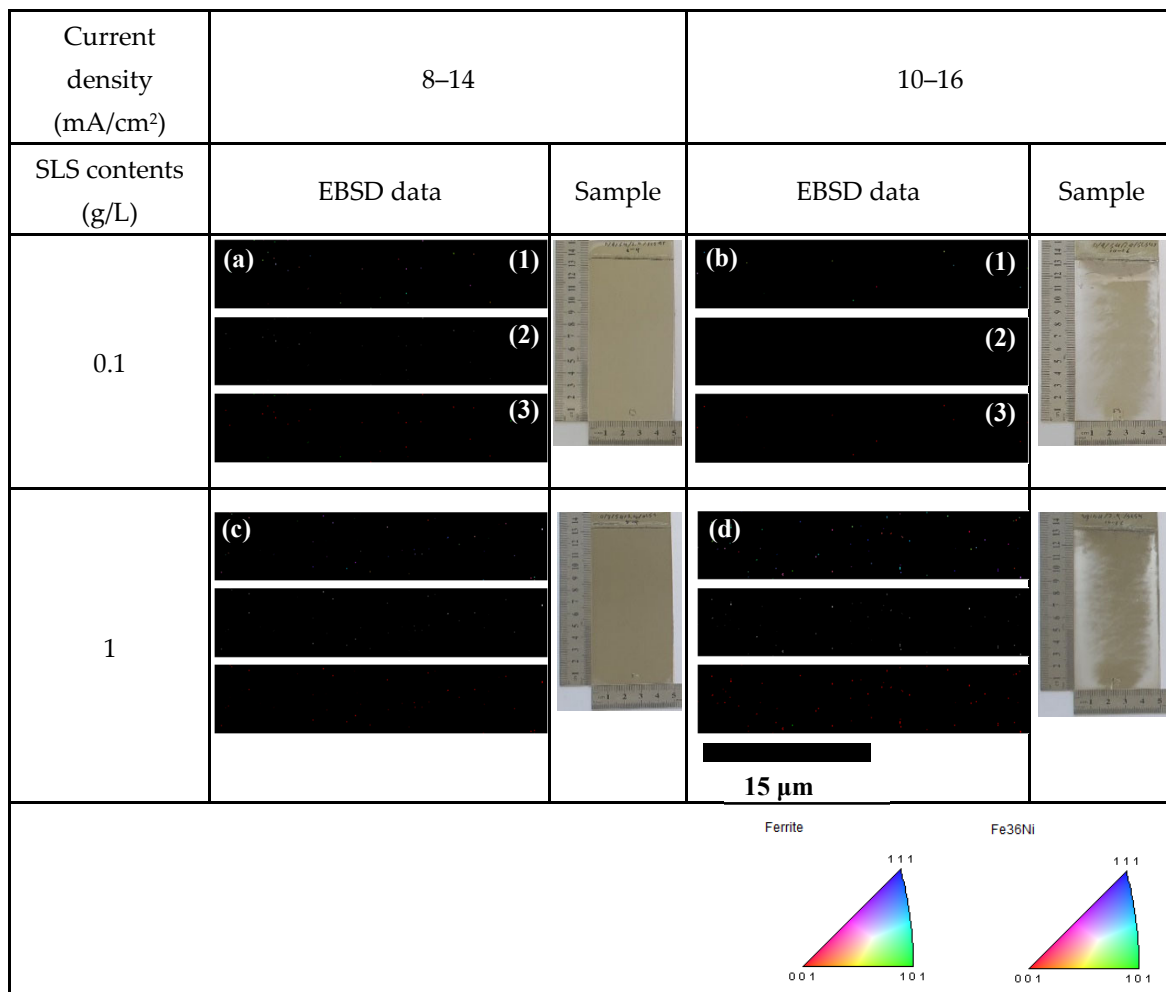
Figure 4. Typical EBSD data containing (1) IPF maps, (2) IQ maps, and (3) phase fraction, and specimen surface at varying SLS contents (g/L) at pH 2.4; (**a,b**) 0.1, (**c,d**) 1.
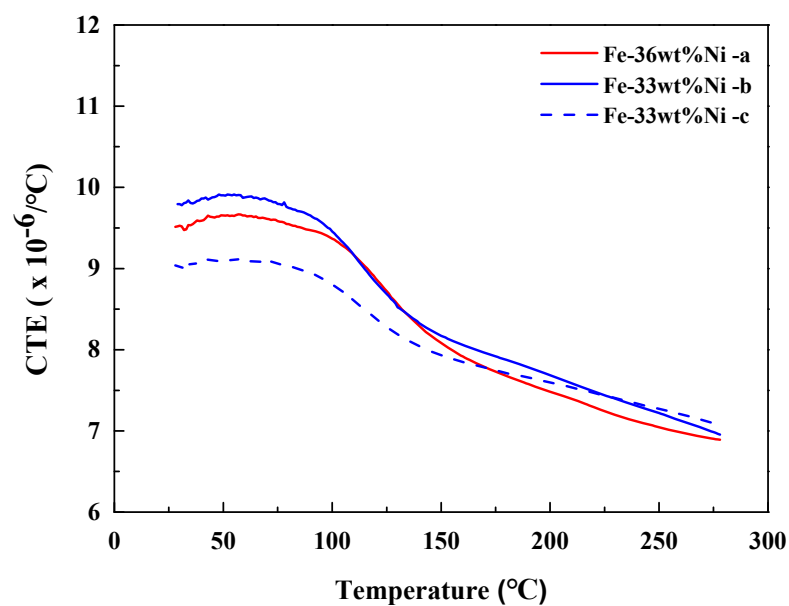
Figure 5. Thermal expansion behavior of the Fe-Ni alloys. CTE versus temperature at varying SLS contents (g/L) at pH 2.4; (a) 0.1, (b,c) 1.

4. Conclusions

The present study investigated how SLS added in electroplating can act as a surfactant and alleviate the difference in surface tension between the plating solution and cathode. The results focused on optimizing the electrodeposition process for manufacturing high-resolution OLED displays with ultra-thin FMM by investigating the impact of SLS content as a surfactant on the properties of electrodeposited Fe-Ni alloys.

(1) To compare whether the amount of SLS added affects the white rust phenomenon, various electroplating conditions were used in combination with the current density (8–14 and 10–16 mA/cm^2) and pH (2.4 and 2.8).

(2) White rust formed on the surface of the sample depending on the amount of SLS content under high pH conditions, and white rust appeared in different amounts depending on the current density under low pH conditions. Under high pH conditions, white rust is formed by a columnar structure, as identified through EBSD analysis. As the SLS content increases, the columnar structure grows and the formation of white rust increases. Under low pH conditions, the white rust is caused by nanograins rather than columnar structure.

(3) The composition according to the difference in the amount of SLS content becomes less uniform as the amount of SLS content increases under high pH conditions, which is consistent with the deepening of the white rust, and the composition for the conditions of 0.1 and 0.2 g/L of SLS addition excludes the electrodeposition composition. Under low pH conditions, the composition was insignificantly changed depending on the difference in the amount of SLS content, and a uniform composition was observed.

(4) The CTE of the electrodeposited sample without white rust is $9.652 \times 10^{-6}/°C$ that is 7.7% lower than that of the sample with white rust, due to the roughness, porosity and Ni element evaporation.

Overall, the optimized conditions were observed at pH 2.4 and a current density of 8–14 mA/cm^2 with an SLS concentration of 1 g/L, which shows the lowest CTE values of $9.101 \times 10^{-6}/°C$ without white rust. This study makes a significant contribution to the literature because this research contributes valuable insights into optimizing the electrodeposition process for advanced OLED displays, offering potential advancements in display technology.

Author Contributions: J.-H.K. wrote the manuscript draft, performed the experiments and validated the data. I.-G.K. performed the experiments and measurements, and revised the manuscript. S.-E.S. wrote the manuscript and analyzed the data. Y.-B.P. designed the project, analyzed the data and revised the manuscript. All authors have read and agreed to the published version of the manuscript.

Funding: This study was supported by the Basic Science Research Program through the National Research Foundation of Korea (NRF) funded by the Ministry of Science, ICT & Future Planning (No. 2021M3H4A3A02098094).

Institutional Review Board Statement: Not applicable.

Informed Consent Statement: Not applicable.

Data Availability Statement: Data are contained within the article.

Conflicts of Interest: The authors declare no conflict of interest.

References

1. Wang, Y.M.; Cheng, S.; Wei, Q.; Ma, E.; Nieh, T.; Hamza, A. Effects of annealing and impurities on tensile properties of electrodeposited nanocrystalline Ni. *Scr. Mater.* **2004**, *51*, 1023–1028. [CrossRef]
2. Park, J.J.; Seo, J.; Yoon, S.; Yoo, B. Electrodeposition of Ni-Fe Alloy in Presence of Complexing Agent. In *ECS Meeting Abstracts MA2022-02*; The Electrochemical Society, Inc.: Pennington, NJ, USA, 2022; p. 950.
3. Nagayama, T.; Ymamoto, T.; Nakamura, T.; Yasushi, M. Fabrication of Low CTE Metal Masks by the Invar Fe–Ni Alloy Electroperforming Process for Large and Fine Pitch OLED Displays. *ECS Trans.* **2013**, *50*, 117. [CrossRef]
4. Nagayama, T.; Yamamoto, T.; Nakamura, T. Thermal expansions and mechanical properties of electrodeposited Fe–Ni alloys in the Invar composition range. *Electrochim. Acta* **2016**, *205*, 178–187. [CrossRef]

5. Tabakovic, I.; Inturi, V.; Thurn, J.; Kief, M. Properties of $Ni_{1-x}Fe_x$ (0.1 < x < 0.9) and Invar (x = 0.64) alloys obtained by electrodeposition. *Electrochim. Acta* **2010**, *55*, 6749–6754.

6. Nagayama, T.; Yamamoto, T.; Nakamura, T. Microstructure Characterization of Electrodeposited Invar Fe-Ni Alloy. In *ECS Meeting Abstracts Prime 2020*; The Electrochemical Society, Inc.: Pennington, NJ, USA, 2020; p. 3827.

7. Park, Y.B.; Kim, I.G. The Gain of Low Thermal Expansivity via Phase Transition in Electroformed Invar. *Coatings* **2018**, *8*, 169. [CrossRef]

8. Torabinejad, V.; Aliofkhazraei, M.; Assareh, S.; Allahyarzadeh, M.; Rouhaghdam, A.S. Electrodeposition of Ni-Fe alloys, composites, and nano coatings—A review. *J. Alloys Compd.* **2017**, *691*, 841–859. [CrossRef]

9. Liu, Y.; Liu, L.; Wu, Z.; Li, J.; Shen, B.; Hu, W. Grain growth and grain size effects on the thermal expansion properties of an electrodeposited Fe–Ni invar alloy. *Scr. Mater.* **2010**, *63*, 359–362. [CrossRef]

10. Naoi, K.; Oura, Y.; Maeda, M.; Nakamura, S. Electrochemistry of Surfactant-Doped Polypyrrole Film(I): Formation of Columnar Structure by ELectropolymerization. *J. Electrochem. Soc.* **1995**, *142*, 417. [CrossRef]

11. Lee, S.-B.; Joeng, K.-H.; Lee, J.-D. Development of Alkaline Degreasing Agent for Electroplating Pretreatment Process. *Appl. Chem. Eng.* **2010**, *21*, 301–305.

12. Michaelis, E.; Wöhrle, D.; Rathousky, J.; Wark, M. Electrodeposition of porous zinc oxide electrodes in the presence of sodium laurylsulfate. *Thin Solid Films* **2006**, *497*, 163–169. [CrossRef]

13. Su, C.-W.; Wang, E.-L.; Zhang, Y.-B.; He, F.-J. $Ni_{1-x}Fe_x$ (0.1 < x < 0.75) alloy foils prepared from a fluorborate bath using electrochemical deposition. *J. Alloys Compd.* **2009**, *474*, 190–194.

14. Oriňáková, R.; Oriňák, A.; Vering, G.; Talian, I.; Smith, R.M.; Arlinghaus, H.F. Influence of pH on the electrolyte deposition of Ni–CO films. *Thin Solid Films* **2008**, *516*, 3045–3050. [CrossRef]

15. Matsui, I.; Uesugi, T.; Takigawa, Y.; Higashi, K. Effect of interstitial carbon on the mechanical properties of electrodeposited bulk nanocrystalline Ni. *Acta Mater.* **2013**, *61*, 3360–3369. [CrossRef]

16. Matsui, I.; Takigawa, Y.; Uesugi, T.; Higashi, K. Enhanced tensile ductility in bulk nanocrystalline nickel electrodeposited by sulfamate bath. *Mater. Lett.* **2011**, *65*, 2351–2353. [CrossRef]

17. Kim, Y.-W.; Joeng, K.-H.; Hong, I.-K. Effect of Current Density on Nickel Surface Treatment Process. *J. Korean Ind. Eng. Chem.* **2008**, *19*, 228–235.